Supporting Information

Intensification of Anodic Charge Transfer from Contaminant Degradation for Efficient H_2 Production

Kai Zhang,[a,d] Gong Zhang,[b] Jiuhui Qu,[b,c] Huijuan Liu*[a,b]

[a] State Key Laboratory of Environmental Aquatic Chemistry, Research Center for Eco-Environmental Sciences, Chinese Academy of Sciences, Beijing 100085, China.

[b] School of Environment, Tsinghua University, Beijing 100084, China

[c] Key Laboratory of Drinking Water Science and Technology, Research Center for Eco-Environmental Sciences, Chinese Academy of Sciences, Beijing 100085, China.

[d] University of Chinese Academy of Sciences, Beijing 100049, China.

E-mail: hjliu@rcees.ac.cn

Supplementary Figures

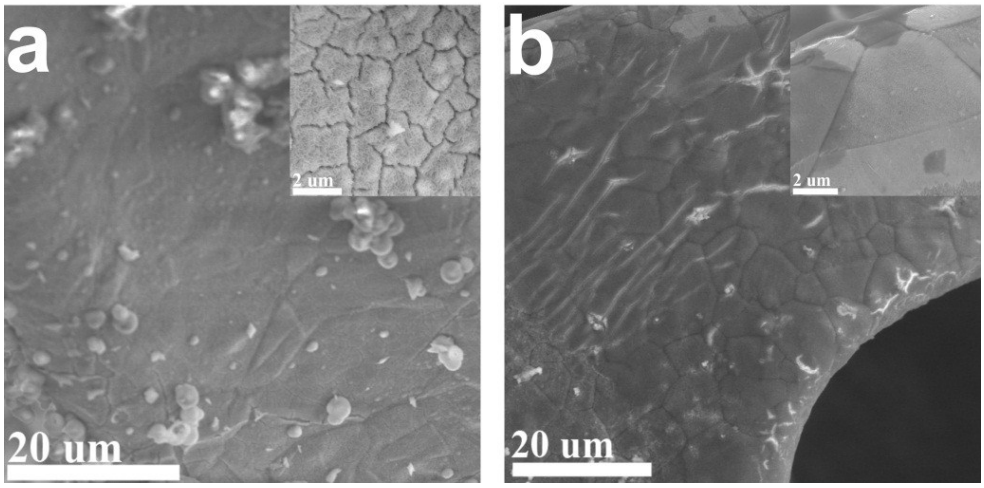

Figure S1. The SEM of the precursors of a) the Mo-Ni_2P and b) the Ni_2P. The precursors of the Mo-Ni_2P were synthesized with the hydrothermal method and the prepared materials included citric acid, Ni sources and Mo sources. In contrast, the precursors of the Ni_2P were also synthesized with the same hydrothermal method, just without Mo sources.

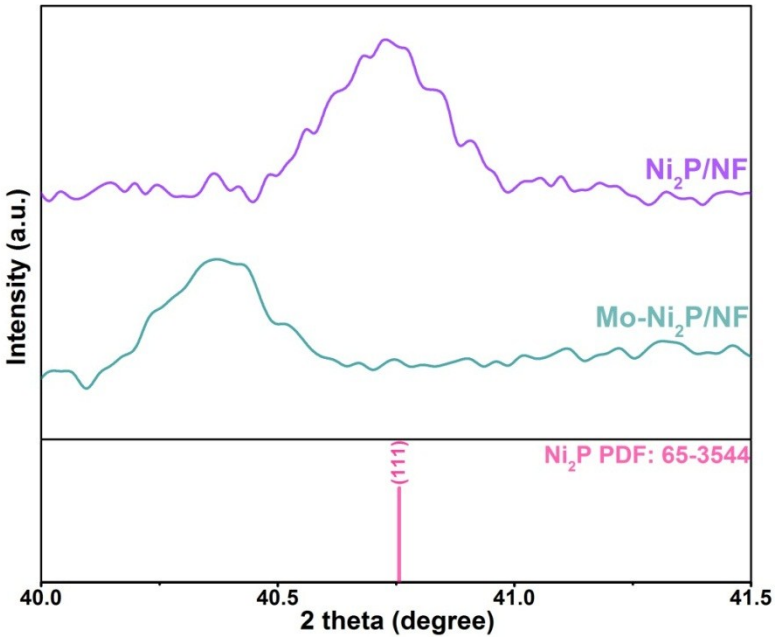

Figure S2. XRD patterns of the zoom-in regions (40-41.5°) of Ni_2P/NF and Mo-Ni_2P/NF.

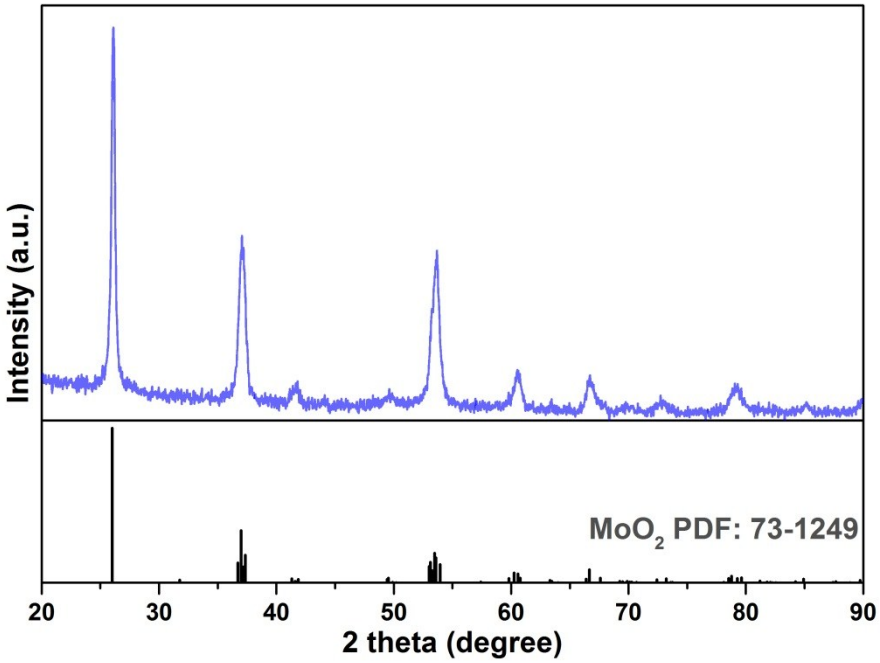

Figure S3. The XRD patterns of the as-prepared Mo. We repeated the experiment without the addition of Ni source for obtaining the Mo materials. The MoO_2 structure indicated that Mo-P bonds could not be formed under 350 °C pyrolysis conditions, excluding the possibility of substitution of Ni by Mo.

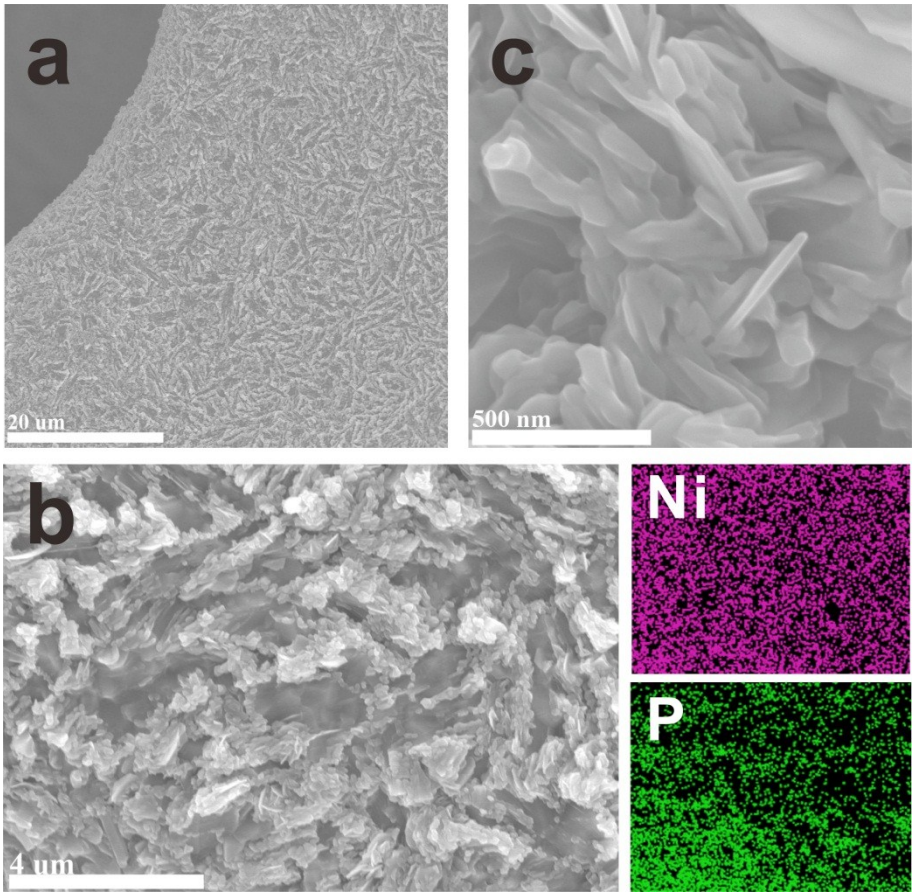

Figure S4. SEM images of Ni_2P /NF at a) low and c) high magnifications. b) SEM and the corresponding elemental mapping of Ni_2P/NF.

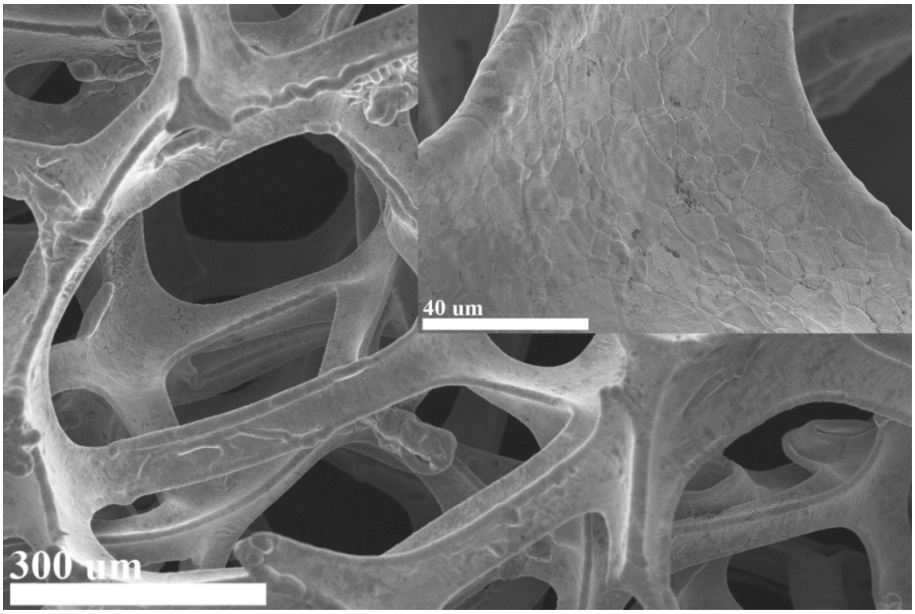

Figure S5. SEM images of pristine Ni foam (NF) at low and (inset) high magnifications.

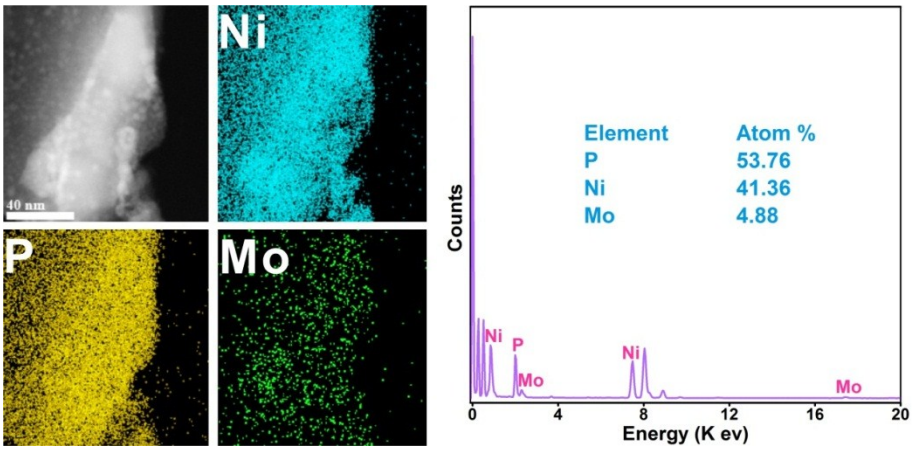

Figure S6. HAADF-STEM image and EDX mapping of Mo-Ni_2P/NF.

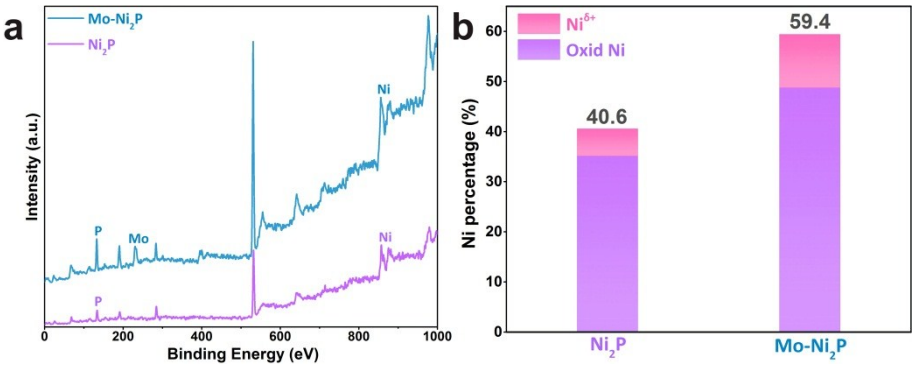

Figure S7. a) XPS survey of Ni_2P /NF and Mo-Ni_2P/NF. b) Surface Ni percentages determined by Figure 2a and Table S2

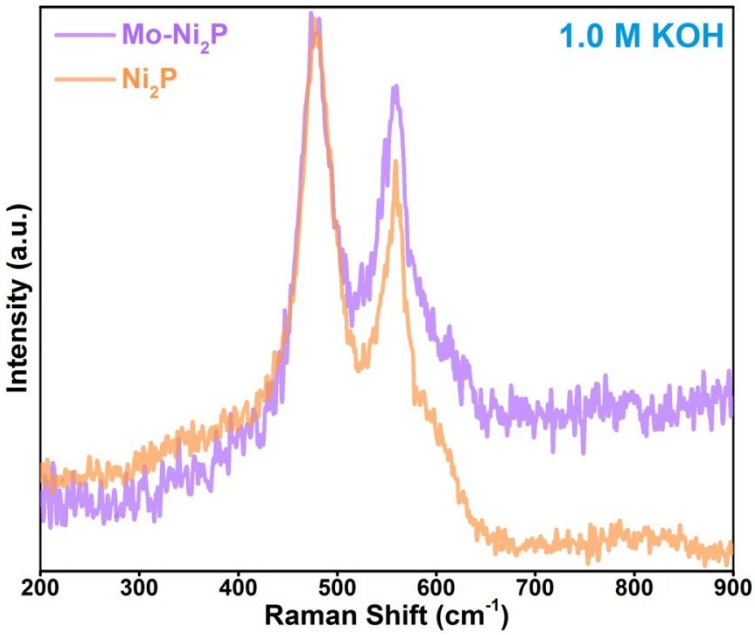

Figure S8. In-situ Raman spectra collected for the Ni_2P and Mo-Ni_2P electrodes at a potential of 0.4 V vs. Ag/AgCl in 1 M KOH solution.

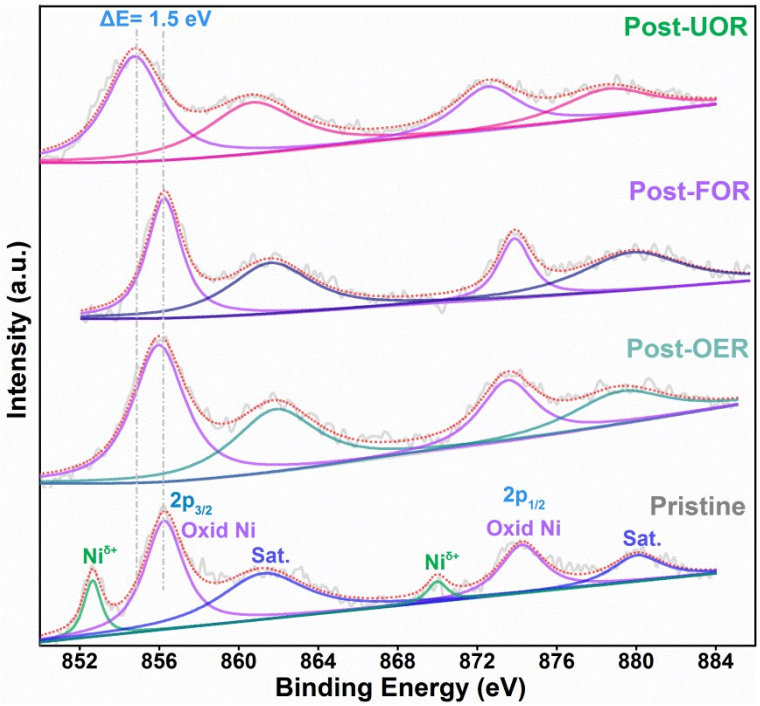

Figure S9. High-resolution XPS spectra of Ni for the pristine, post-OER, post-FOR, and post-UOR Mo-Ni_2P/NF samples

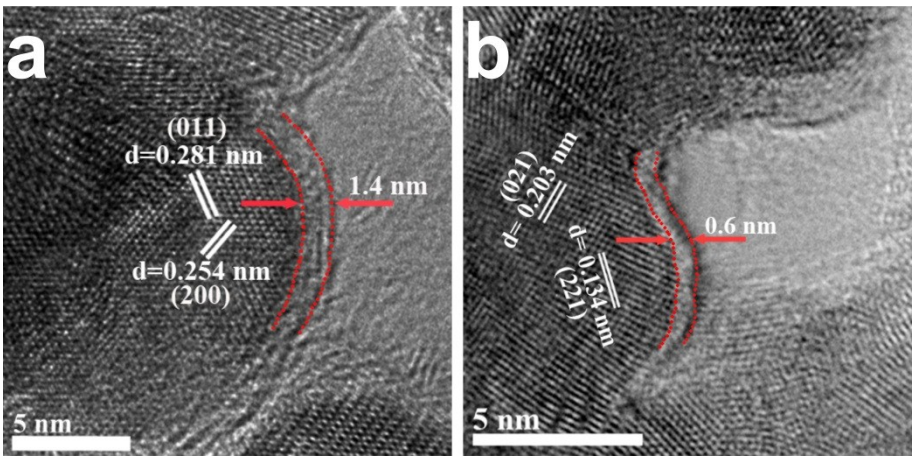

Figure S10. HRTEM images of Mo-Ni_2P/NF sample after a) FOR and b) UOR electrolysis.

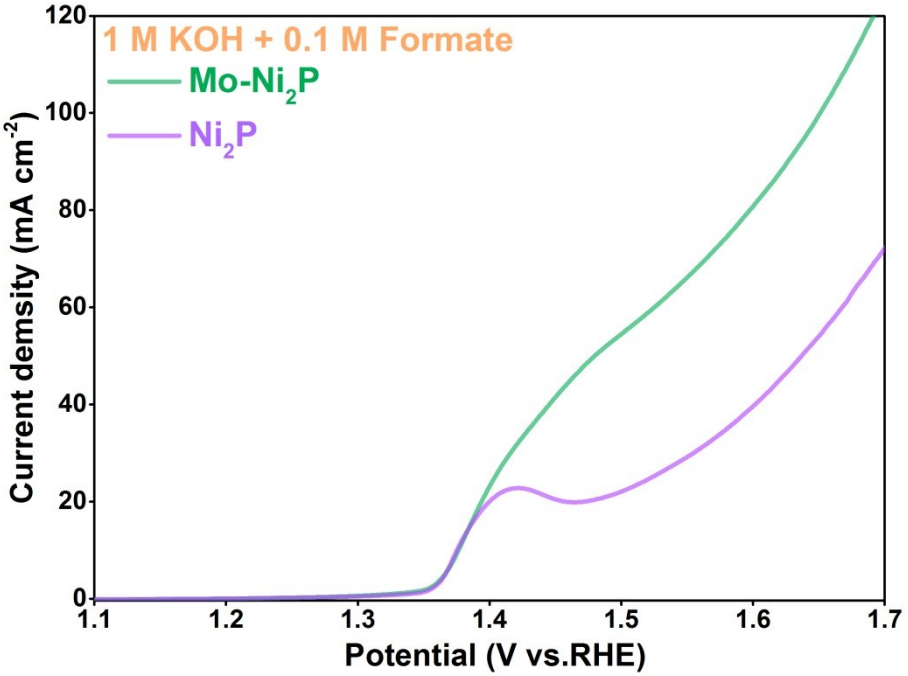

Figure S11. Linear sweep voltammetry (LSV) plots of Mo-Ni_2P/NF and Ni_2P/NF, respectively, in 1 M KOH electrolyte with 0.1 M formate.

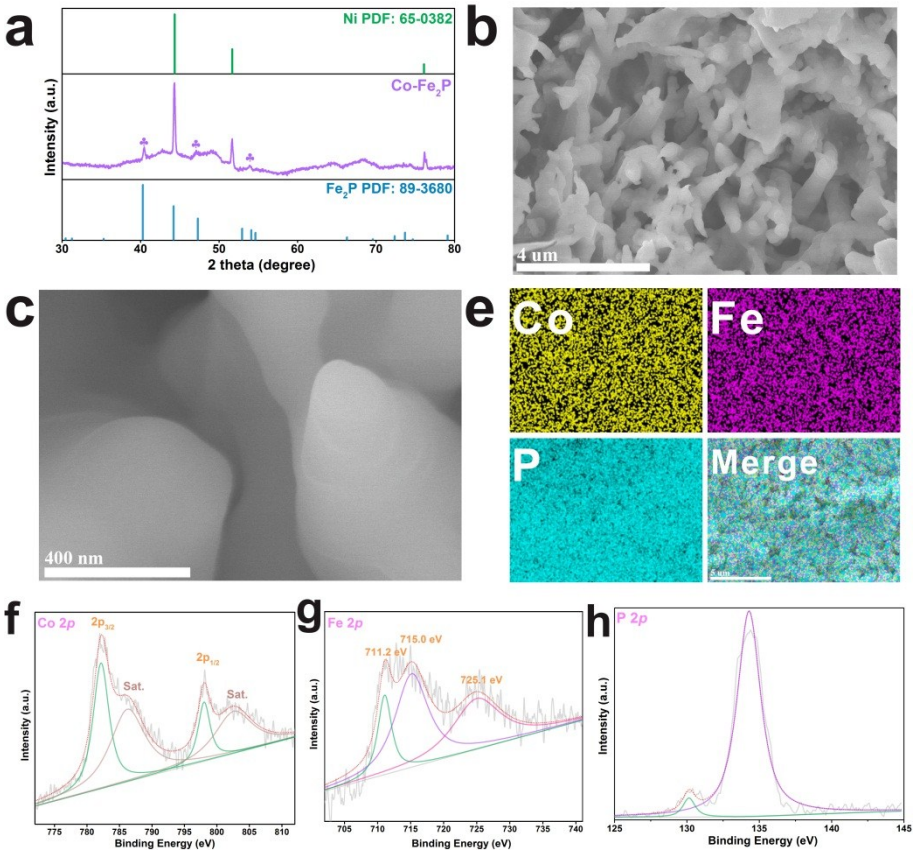

Figure S12. a) XRD patterns of Co-Fe_2P/NF /NF. b, c) SEM images of Co-Fe_2P/NF electrode. e) element mapping of Co, Fe and P. f-h) High-resolution XPS spectrum of Co 2p, Fe 2p, and P 2p for the Co-Fe_2P/NF.

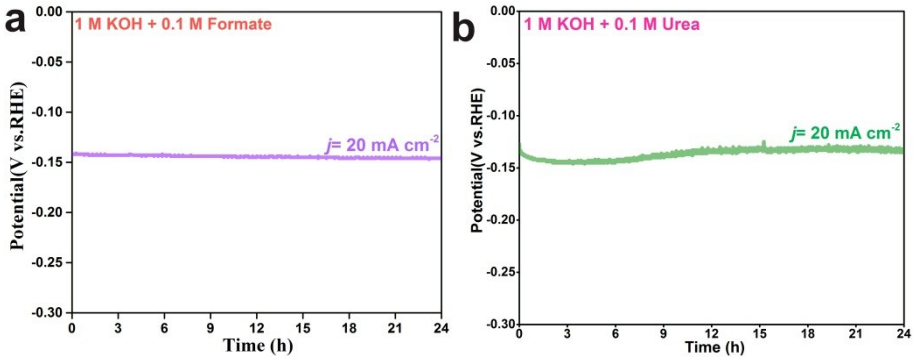

Figure S13. Chronopotentiometric curve of Mo-Ni_2P/NF for H_2 evolution at -20 mA cm^{-2} in 1.0 M KOH containing 0.1 M formate and 0.1 M urea.

Figure S14. Digital images to show the Mo-Ni_2P/NF (+) || Co-Fe_2P/NF (−) urea electrolyzer powered by a single cell AAA battery with a nominal voltage of 1.5 V for UOR.

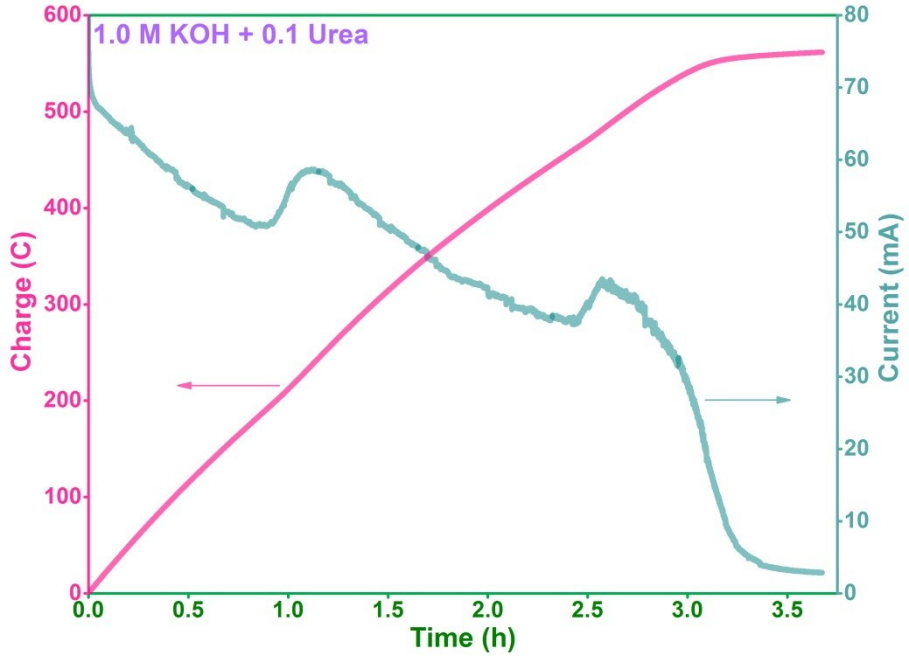

Figure S15. Controlled potential electrolysis of Mo-Ni_2P/NF in 1.0 M KOH containing 0.1 M urea at a potential of 1.48 V vs RHE.

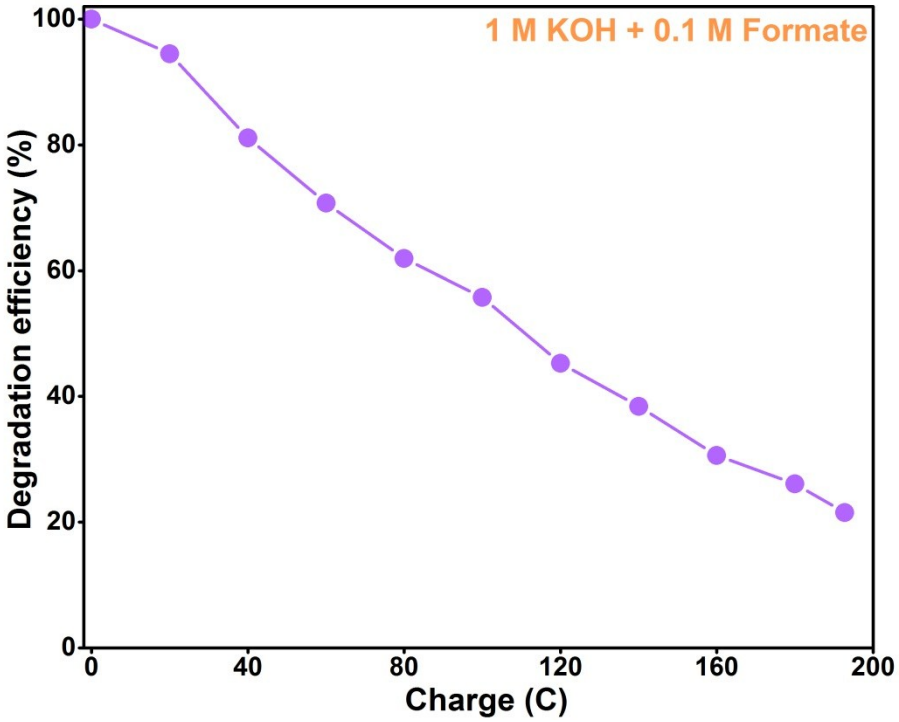

Figure S16. Degradation (%) changes of formate for Mo-Ni_2P/NF at 1.48 V vs. RHE in 1.0 m KOH with 0.1 M formate.

Supplementary Tables

Table S1. Composition of the Mo-Ni_2P used in our experiment

Element	Atom (%)[a]
Mo	5.12
Ni	41.35
P	53.53

[a]Data was calculated from the result of ICP-OES.

Table S2. Fitting parameters (peak position, peak area and species percentage) for both Ni $2p_{3/2}$ and Ni $2p_{1/2}$ profiles taken on Mo-Ni_2P and Ni_2P

Samples	species	B.E.(eV)		area		Ni percentage (%)
		$2p_{3/2}$	$2p_{1/2}$	$2p_{3/2}$	$2p_{1/2}$	
Mo-Ni_2P	$Ni^{\delta+}$	852.6	870.0	309	127	59.4
	Oxid Ni	856.2	874.2	1323	658	
	Sat	861.2	880.0	1239	412	
Ni_2P	$Ni^{\delta+}$	853.0	870.0	65	60	40.5
	Oxid Ni	857.0	875.0	482	318	
	Sat	862.0	880.0	845	510	